Intrinsic time resolution and efficiency study
for simulated scintillators plastics with Geant4

E. Márquez Quintos[a], C. H. Zepeda Fernández[a,b], L. F. Rebolledo-Herrera[a], and E. Moreno Barbosa[a,*]

[a]Facultad de Ciencias Físico Matemáticas, Benemérita Universidad Autónoma de Puebla,
Av. San Claudio y 18 Sur, Ciudad Universitaria 72570, Puebla, México.
[*]e-mail: emoreno@fcfm.buap.mx
[b]Cátedra CONACyT, 03940, CdMx México.

The time resolution (TR) is one of the most important characteristic of a detector. The particular case of a scintillator, the collection of light also is important, it depends of the sensitive area of the photo-sensor (*Scorer*). Normally, the Scorer of Photomultipliers Tubes (PMTs) is greater than the Scorer of Silicon Photomultipliers (SiPMs). Other differences are the voltage of operation, their size and cost, in some cases, the large size of PMTs can be difficult to place, if small space is required, in which case, it is preferable to use SiPMs. The value of TR also depends of the size and geometry of the scintillator, number of photo-sensors and the electronic part.

In this work, we study the mean optical photon arrival time distribution (AT) to a Scorer from a SiPM of 6×6 mm^2. We define the variation of AT as *the intrinsic time resolution* (ITR). In Geant4, we simulated two different geometries: square and hexagonal, for a BC-404 plastic scintillator coupled to one Scorer. The sources simulated were Sr^{90}, Co^{60}, Cs^{137}, Na^{22} and μ^- of 1 GeV. It is shown that AT and ITR depends of the geometry and size of the plastic scintillator, the location of the Scorer, the incident particle and its energy. Then, the ITR and therefore the TR is not a constant for a detector. Finally, we show the relation between AT and the deposited energy by the particle incident, which are related in the experiment to the response time event of the detector and the deposited charge by the incident particle, respectively.

Keywords: Time resolution; scintillator plastic; photosensor; optics photons.

1. Introduction

One of the most important characteristic for a detector is the time resolution (TR), many works have been done to improve it [1]. For the case of the scintillator materials, the detection of optical photons is important to obtain the signal, where, photo-sensors are used, then, the detection area (*Scorer*) is important, if it is bigger, it has better light collection. Two kind of photo-sensors are commonly used: the Photon Multiplier Tube (PMT) and Silicon Photon Multiplier (SiPM). The PMTs have larger dimensions than SiPMs, which have a size of the order of cm, while SiPMs have a size of mm. Therefore, geometrically PMTs have a larger Scorer than SiPMs. However, when it is required to work with a small plastic scintillator (mm^3) using a SiPM is more convenient, due to its Scorer [2]. Recently, the use of SiPMs have been used more than PMTs by getting a better response and signal [4–6]. A 6×6 mm^3 SensL SiPM has two kind of output signals: the *standard* and *fast* [7]. The fast signal pulse has a rise time of 1 ns and a pulse width of 3.2 ns, while, the rise time of the standard signal pulse is 4 ns and a width of 100 ns. From the standard pulse, it is possible to reconstruct the deposited charge, making an integration of it, for this reason, reading this pulse gives physical information. However, recently, it has been shown that the deposited charge can be reconstructed from the fast signal [8]. Therefore, this signal can be taken for a higher detector response, due to its rise time and improve the TR value.

Usually crystals or plastics are used in scintillation detectors, depending on the particles to be detected, it is chosen which one to use. Recently, with the aim to improve the time and spatial resolution, the coupling between SiPM and scintillator material has been widely investigated [9, 12]. The plastic scintillators have been more frequently used due to their ease of fabrication in different geometries. In particular, the BC404 plastic scintillator is proposed for the construction of a new Mexican detector [2] within the Multi Purpose Detector experiment at the Nuclotron Ion Collider fAcility (NICA) [3]. The detector simulations is an important study, mainly to have a control on the physical parameters as optical arrival time, interaction point, etc. One of this software is GEANT4 [13, 14]. As it was mentioned above, the use of SiPMs has shown some advantages when reading the signal and, simulations in this field have been developed [15–18].

We define the *intrinsic time resolution* (ITR) by the standard deviation of the *mean of the optical photon arrival time distribution* (AT) to the Scorer. Then, the ITR is an intrinsic property which depends of the geometry, scintillator and Scorer sizes, but also the scorer location attached to the scintillator. The number of Scorers also modifies the value of ITR, in particular for its improvement [1]. In the experiment, the TR (σ_{TR}) is measured and its relation with the ITR (σ_{ITR}) is,

$$\sigma_{TR}^2 = \sigma_{ITR}^2 + \sigma_{ele}^2 + \sigma_{ref}^2. \tag{1}$$

Where σ_{ele} and σ_{ref} are the time resolution of the electronics and the reference trigger detector, respectively [1].

In this work, we show the value of ITR and AT as function of the BC404 plastic scintillator size and the location of the Scorer, as well as the incident particles and their energy. Finally, we show an estimate result in the experimental measurements.

2.   Simulation methodology

The Geant4 10.7 [19] was used for this simulation. All optical properties for the BC-404 plastic scintillator were considered as it is described below.

2.1.   Plastic scintillator BC-404 simulation

The polyvinyltoluene material for BC-404 plastic scintillator is already defined in the environment of Geant4 by *G4_PLASTIC_SC_VINYLTOLUENE*. All the optical properties used for the simulation have been taken from the Saint Gobain BC-404 data sheet [20] and the Light output property was taken from a thesis study [21]. Some of these optical properties are shown in Table I. The emission spectra simulated based is shown in Fig. 1.

2.2.   Optical photons simulations

The Geant4 environment models major optical physics in detector. It includes process as ionization, Compton, photoelectric, scintillation, Cerenkov and the resulting optical photon propagation [22]. The main information for this work is from the optical photons, which are counted by the hits on the Scorer surface (see 2.4).

TABLE I. Optical properties for the simulation of BC-404 plastic scintillator.

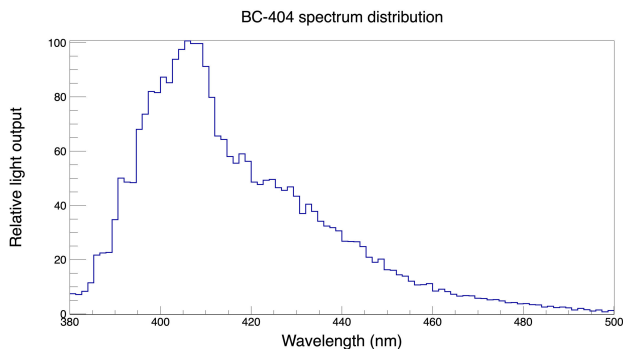| Light output (photons /MeV)	Refraction index	Light length (m) attenuation	Wavelength of Max. Emission (nm)
10,880	1.58	1.4	408

FIGURE 1. BC-404 plastic scintillator emission spectra simulation.

TABLE II. Particle and energy simulated for each source.

Source	Particle	Energy (MeV)
Na^{22}	γ	0.511
	γ	1.275
Cs^{137}	γ	0.6617
Co^{60}	γ	1.170
Sr^{90}	e^-	0.546
μ^-	μ^-	1,000

2.3.   Sources simulation

Five radiation sources were simulated: Na^{22}, Cs^{137}, Co^{60}, Sr^{90} and μ^-. The first four sources belong to a kit that can be found in laboratories [23] and for this study, it is considered their main branching ratio decay [24–27]. The μ^- particles are considered as a cosmic ray average. Based on these specifications the particles and energy for each source are shown in Table II. For the next sections, we refer as *source* for the kit sources and μ^- *source* for the muon. For each source 6,000 events were considered, where a single event is understood as a particle from the source which interacts with the BC-404 scintillator. Finally, the particles were concentrated in a radius of 2 mm, considering the effective aperture of the kit source and located at the geometrical center of each geometry configuration and one millimeter away from its surface.

2.4.   Configuration simulation

We simulated two geometries for the BC-404 plastic scintillator:

- A square geometry with a front face area of 20 × 20 mm² and a width of 3 mm (square configuration).

- A hexagonal geometry with 50 mm high and 20 mm wide. For this geometry we considered two arrangements.

  – The Scorer coupled on one of the hexagonal faces at the geometrical center (first configuration).

  – The Scorer coupled at the center on one of the side faces (second configuration).

These configurations are shown in Fig. 2, the interaction point was simulated on the geometrical center of each geometry and located at 1 mm from the plastic scintillator. The Scorer was simulated with 6 × 6 mm², which represents a SensL SiPM of this size as already mentioned. The configuration in which the Scorer located on the lateral face of the square geometry was not considered, due to its small width. The width of the Scorer is not relevant considering the reasons explained in Sec. 2.5.

Finally, all the optical photons physical parameters as energy, arrival position and arrival time were obtained on the
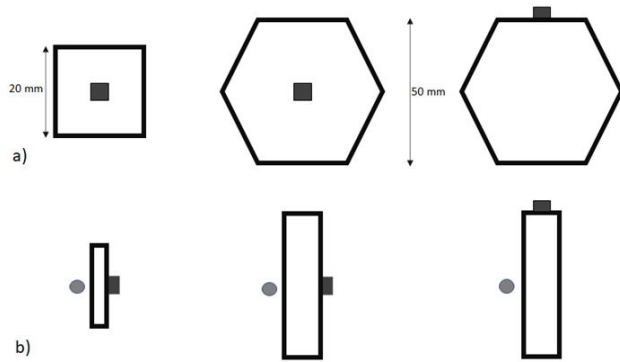
FIGURE 2. Illustration for the three configurations. a) front view and b) side view. The square and hexagon represent the BC-404 plastic scintillator, the solid square represents the Scorer, and the solid circle represents the point of interaction.

Scorer surface. In addition, the deposited energy of the incident particle was saved and obtained in the BC-404 scintillator. This last quantity was used to obtain an estimation of the experimentral measurement (see 3.3).

2.5. Optical boundaries

The environment surrounding the plastic scintillator and the scorer was considered air by the material giving in Geant4: *G4_Air*. For this study are considered two boundary condition:

- Scintillator-environment: It is considered with 95% efficiency in reflection from the scintillator to environment surface. The plastic scintillator surface was considered polished. Finally, the interface was considered by dielectric-metal. As we are not interested in the optical photons that come out of the scintillator, this condition is enough.

- Scintillator-Scorer: This surface was considered 100% absorbent, in order that the optical photons that arrive to the Scorer, are not reflected and therefore do not count them more than once. Then, the interface is not relevant and it was considered by dielectric-metal, dielectric by scintillator and metal for the scorer. As the optical photons do not pass through the Scorer, its width is not important.

2.6. Intrinsic time resolution methodology

To obtain the ITR of each configuration, we obtained the AT value, this value represents the average time at which the optical photons reach to the Scorer and it is obtained event by event. Finally, we obtained the fit Gaussian distribution from the set of all mean values to obtain the σ parameter, which it represents the ITR. This technique has been compared with the experiment [1] and also is used to calculate the ITR for the MiniBeBe detector (described in the Sec. 6 in Ref. [2]).

2.7. Intrinsic efficiency

We define the intrinsic efficiency (ϵ_I) of a detector as:

$$\epsilon_I = \frac{N_d}{N_c}, \tag{2}$$

where N_d is the number of optical photons detected on a Scorer and N_c is the number of optical photos created. Analogously to ITR, ϵ_I depends of the size and geometry of the plastic scintillator and the location and size of the Scorer. Then, to obtain a ϵ_I value close to one, it is necessary to line the scintillator with highly reflective and light-insulating material.

3. Results and analysis

A plastic scintillator (in this case BC-404 [20]) is not particularly efficient for γ-particles detection in which case crystal scintillator is more often used [28], due to the atomic number of the material and this effect was observed during simulation, where it was obtained that:

- In the square geometry: for fifty γ-particles, in average, one of them interacts with the plastic scintillator.

- In the hexagonal geometry: for fifty γ-particles, in average, two of them interacts with the plastic scintillator.

This difference in interaction is due to the width, for the square configuration the particles have a shorter interaction distance compared with the width of the hexagonal configurations.

For the e^- and μ^- particles we obtained non-null events for all configurations.

3.1. Square geometry

To exemplify, the AT distribution is shown for the case of Sr^{90} in Fig. 3, where the mean value of 12.28 ± 0.03 ps and an ITR value of 1.88 ± 0.01 ps were obtained. We obtained the distribution values for the other sources and configurations, the results are shown in Figs. 4 and 5. Due to the small size of the plastic, the ITR values for all sources are consis-
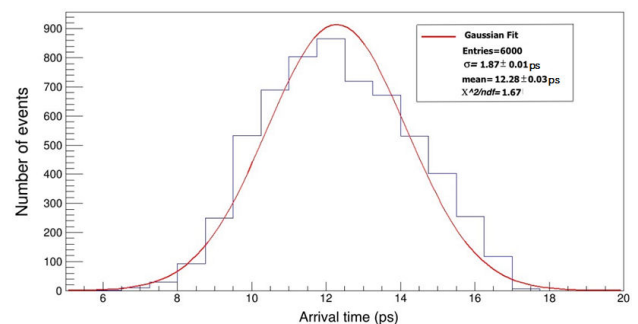

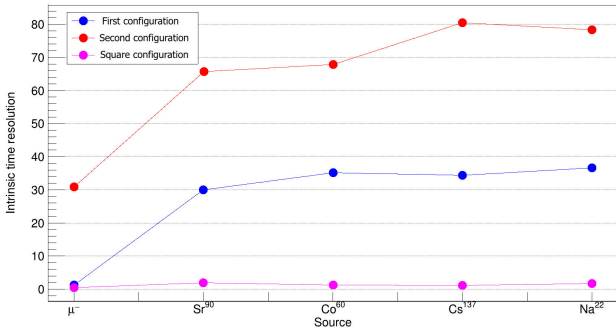FIGURE 3. The mean arrival time optical photon distribution for all events of Sr^{90}.

FIGURE 4. The ITR values for all configurations.

tent around 2 ps. The mean values (except for Sr^{90}) are consistent for all sources around 2 ps. These constant values are due to the small dimensions of the plastic scintillator, where the optical path is small [29]. The mean value for the Sr^{90} source is 12.26±0.02 ps, it will be discussed in the next subsection. For larger dimensions the ITR and AT change as it is shown below.

3.2. Hexagonal geometry

Once again, to exemplify the AT, in Fig. 6 are shown the distribution for Sr^{90} source, considering both hexagonal configurations, getting an ITR value of $\sigma = 29.92 \pm 0.29$ ps and $\sigma = 65.75 \pm 0.73$ ps for the first and second configuration, respectively. The same results are obtained for the rest of the sources, as it is shown in Fig. 4. It can be seen that the ITR is greater for the second configuration than the first configuration for all sources. This is due to the mean arrival time, resulting that the optical path to arrive to the Scorer is greater for the second configuration than the first configuration, as it is shown in Fig. 5, it can be observed that for the second configuration the optical photons take longer time to arrive at Scorer than the first configuration, therefore the σ value also is greater. The case of μ^- source has the lowest values for mean and σ, this is due to its great energy, by which more optical photons are created.

According to Table II, the Sr^{90} source has similar energy than the rest of the sources, however, it has mass different from zero. As a consequence of these characteristics the e^- is stopped at a certain depth, as it is shown in Fig. 7 for all
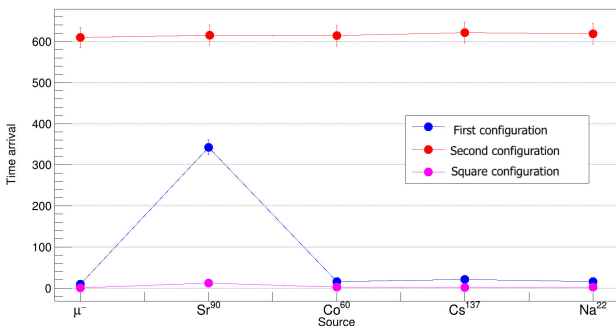

FIGURE 5. The mean arrival time optical photon is shown for all sources.
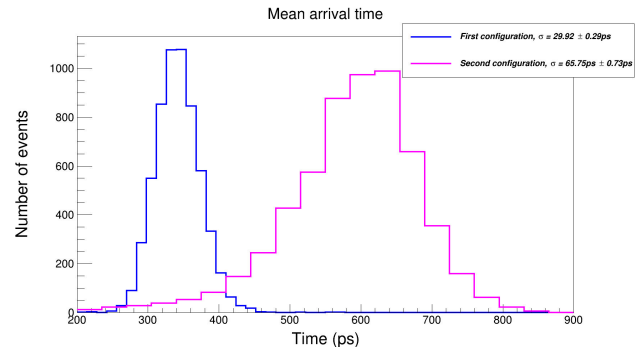

FIGURE 6. The mean arrival time optical photon distribution for Sr^{90} source for the Scorer located at center (blue-line) and located at top (magenta-line).
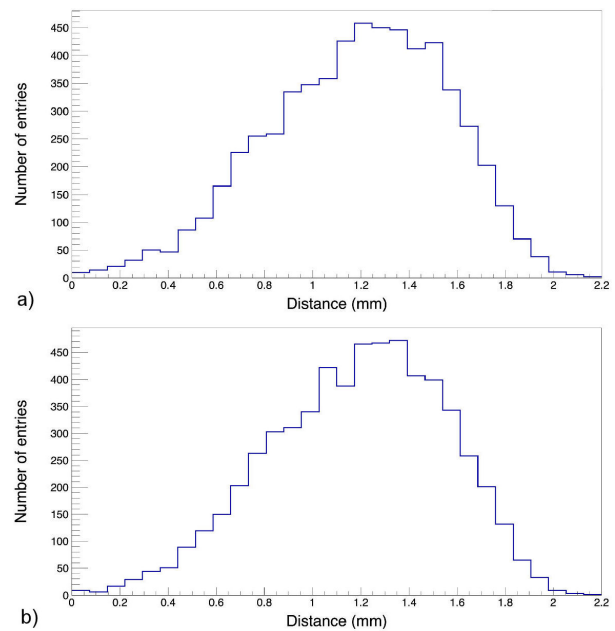

FIGURE 7. The depth reached by the e^- emitted by Sr^{90} source in the hexagonal a) and square b) geometry.

configurations. It can be noted that the depth is the same, because the same material is used. For the hexagonal configurations (both), the e^- is stopped at 10% of the width, therefore, very few photons are created compared with the other sources, which go through the plastic and therefore create photons on their way. The optical photons produced by the Sr^{90} in the first configuration travel a greater optical path and therefore the mean arrival time is greater as it can been seen in Fig. 5. For the second configuration, the mean arrival time for the Sr^{90} is consistent with the other sources, due to the location of the Scorer, so the optical path is almost the same. For the case of the square configuration, it can been seen that the mean arrival time is slightly bigger, for this case the e^- is stopped at 73.3% of the width, once again the optical path is greater, however, the difference with the optical path of optical photons produced by the other sources it is not that big compared to hexagonal configurations.

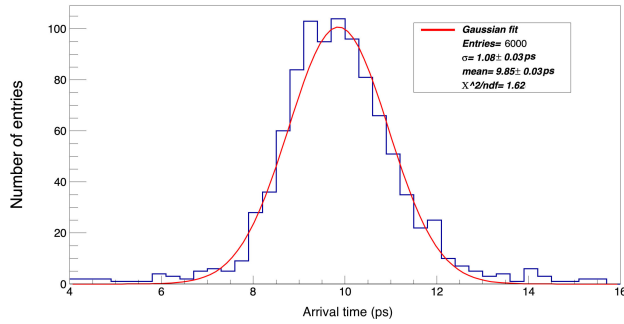FIGURE 9. Intrinsic efficiency values for all configurations.

FIGURE 8. Arrival time optical photons distribution produced by μ^- interacting to the first configuration.

For the hexagonal configurations the μ^- source, that although it is a massive particle, has the smaller ITR value, this is due to the greater energy of the particle, which its interaction with the BC-404 scintillator produces much more optical photons and therefore the variation of the values around the mean (ITR) is smaller. To show this trend, as an example in Fig. 8 is shown the AT for the first configuration.
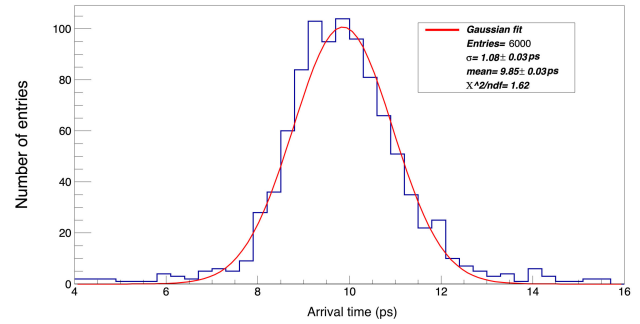
In Fig. 9 is shown the ϵ_I values for all configurations and sources. Clearly, The square configuration has the best ϵ_I value and having better values for the other two configurations. This phenomenon is due to the optical path, that for the case of the square configuration, it is less than the hexagonal, then, the light attenuation becomes a relevant quantity for the hexagonal configuration due to its volume. Finally, the location of the Scorer also influences as it can be seen for the first and second configuration. The effect of the depth for the Sr^{90} source is reflected for second and square configurations.
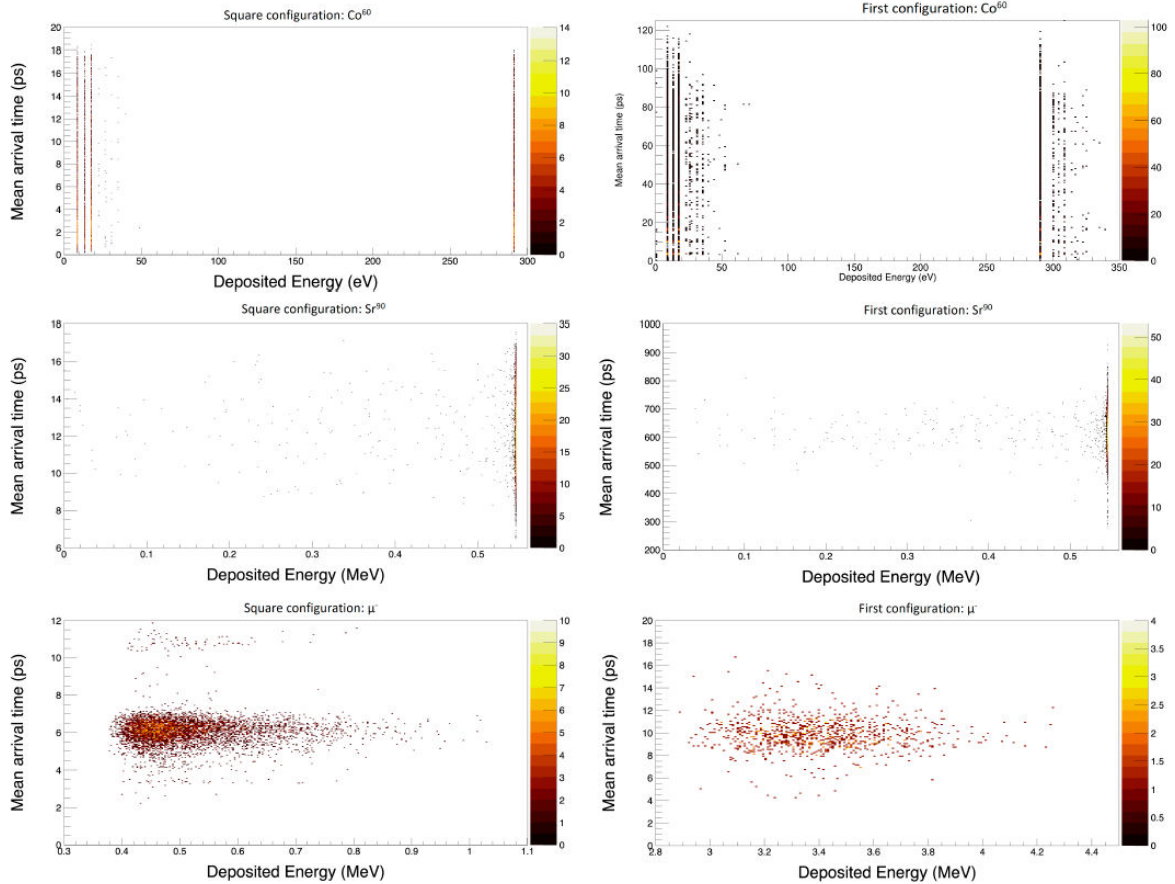

FIGURE 10. Relation between mean arrival time and deposited energy for square configuration (left) and first configuration (right) for Co^{60} (top row), Sr^{90} (middle row) and μ^- (down row) sources.

3.3. Experimental measurement estimation

The deposited energy (E_{dep}) by the incident particle is related and increases or decreases with the charge deposited, which can be obtained from the pulse of the photo-senor [8]. For the case where it is required to measure simultaneously the deposited charge and the response time of the detector, it is commonly used a Quad Digital Channel (QDC) and a Time to Digital Convert (TDC), respectively, to make a scatter plot. The AT is related to the TDC value, as it is shown in Eq. (1). Then, the relation of AT and E_{dep} is related to the values of TDC and QDC. As an example, in Fig. 10 are shown the AT and E_{dep} relations for the Co^{60}, Sr^{90} and μ^- sources, for the case of square and first configuration.

As it was mentioned above, the γ particles hardly interact with plastic, for which an order of eV in E_{dep} is obtained, also due to the nature of the particle, a quantified E_{dep} is obtained. Also, it can be seen the effect that occurs with the electron, which does not pass through the plastic scintillator and therefore deposits all its energy. Finally, the μ^- source deposits more energy in hexagonal configurations than in square configuration, due to the width of the hexagon, in which, it interacts more. Similar relations to Co^{60} were obtained for the Na^{22} and Cs^{137} sources. For the second configuration we also obtained similar relations, having AT values greater than in the first configuration.

4. Conclusions and discussion

In this work we have shown that ITR and, therefore, the TR are not constant, that is, they depend of the energy, type of particle, the interaction point, the location of the Scorer (also the number of them [1]) and the size and geometry of the plastic scintillator. The BC-404 plastic scintillator of small size exhibits an ITR close to 2 ps, which is also independent of the number of scorers [2]. While for a big size, the ITR and TR vary and in particular increase compare with a small size.

Another characteristic for a scintillator detector that should also be considered is the AT. This quantity also de-

pends on the features mentioned above. While the ITR can be similar or consistent for the kit source, the AT varies for Sr^{90}, due to the energy of the e^-, which does not pass through the material, therefore, this source is detected in a longer time than the rest of the kit sources.

Finally, the last characteristic that we propose for a detector is the intrinsic efficiency, which, allows to know the amount of optical photons detected by the configuration and geometry of a detector and the incident particle.

The low ITR values for the square configuration can be complicated to measure with conventional equipment, however, recently a TDC has been developed, whose RMS is of 2.2 ps [30]. The ITR value for the hexagonal configurations is more accessible to observe in a laboratory. The results obtained in this work are consistent with the results obtained in [1], which the incident particles were π^+ of 0.5 GeV and from which a ITR of 45 ps was obtained.

From these results it is simple to note that the square geometry can be used in the Mini-BeBe detector, which requires a temporal resolution less than 100 ps, with the purpose of working as a level 0 trigger for the TOF detector of NICA-MPD [2].

Previously, a ITR analys was made for the second configuration [1], from these results, we confirm that the ITR value is different depending on the type of particle and energy. One of the hexagonal configurations will be implemented in the BeBe detector, in which, a low value of the ITR and the TR is not important for its purpose [31].

These configurations can also be used in a miniPET. Recently, the use of plastic scintillators in this divice is used [32], however, it is used bigger size of plastic scintillators, obtaining a bigger ITR and TR values, as well as, obtaining a bigger value of spatial resolution. Using the configurations studied in this work, these values can be improved.

These simulations were made in order that they can be carried out in the laboratory, when using the kit sources. By using a TDC and a QDC, the shape of the Fig. 10 can be recreated. In fact, the intrinsic efficiency also can be calculated.

1. M. Alvarado *et al.*, A beam-beam monitoring detector for the MPD experiment at NICA, *Nucl. Instrum. Methods Phys. Res. A* **953** (2020). `https://doi.org/10.1016/j.nima.2019.163150`.

2. R. Acevedo Kado *et al.*, The conceptual design of the miniBeBe detector proposed for NICA-MPD *JINST* **16** (2021) P02002.

3. V. Golovatyuk, V. Kekelidze, V. Kolesnikov, O. Rogachevsky, A. Sorin, The Multi-Purpose Detector (MPD) of the collider experiment, *Eur.Phys. J.* **A52** (2016) 212, `doi:10.1140/epja/i2016-16212-1`.

4. E. Garutti, Silicon Photomultipliers for High Energy Physics Detectors, *JINST* **6** C10003 [arXiv:1108.3166].

5. F. Simon, Silicon Photomultipliers in Particle and Nuclear Physics, *Nucl. Instrum. Meth.* **A 926** (2019) 85, [arXiv:1811.03877].

6. K.E. Kuper, V.P. Oleynikov, V.V. Porosev, G.A. Savinov and W. Drozdowski, On reachable energy resolution of SiPM based scintillation counters for X-ray detection, *JINST* **12** (2017) P01001.

7. SensL Technologies Ltd., *Product Selection Guide* (2013), `http://sensl.com/products`.

8. C. H. Zepeda-Fernández *et al.*, Electric charge estimation using a SensL SiPM *JINST* **15** (2020) P09008. `https://doi.org/10.1088/1748-0221/15/09/P09008`.

9. E. Ebru and C. Celiktas, Effects of the positions of scintillation detectors with fast scintillators and photomultiplier tubes on TOF-PET performance, *Pramana* **94** (2020) 27.

10. W. Krzemien *et al.*, A novel TOF-PET detector based on plastic scintillators, *IEEE Nucl. Sci. Symp. Med. Imag. Conf. (NSS/MIC) 2015* (2015) 1.

11. L. Raczynski, Reconstruction of signal in plastic scintillator of PET using Tikhonov regularization, *IEEE Eng. Med. Biol. Soc. Ann. Int. Conf. 2015* (2015) 1.

12. A. Wieczorek *et al.*, Novel scintillating material 2-(4-styrylphenyl)benzoxazole for the fully digital and MRI compatible J-PET tomograph based on plastic scintillators, *PLoS One* **12** (2017) e0186728.

13. R. Ghadiri and J. Khorsandi Studying the response of a plastic scintillator to gamma rays using the Geant4 Monte Carlo code *Applied Radiation and Isotopes* **99** (2015). `https://doi.org/10.1016/j.apradiso.2015.02.017`.

14. U. Zafar, *Light output simulation of LYSO single crystal.* `arXiv:1305.3010[physics.ins-det]` **99** (2015).

15. E Leming *et al.*, A GEANT4 Monte Carlo simulation to describe the time response of a coupled SiPM and LYSO detection system. *JINST* **9** (2014) C06008,

16. Xi Daoming *et al.*, Optimization of the SiPM Pixel Size for a Monolithic PET Detector. *Physics Procedia* **37** (2012).

17. W. Joshua, Cates and Craig S Levin Evaluation of a clinical TOF-PET detector design that achieves ≤100 ps coincidence time resolution *Phys. Med. Biol.* **63** (2018) 11.

18. N. Otte *et al.*, *The SiPM - A new Photon Detector for PET*, *Nuclear Physics B - Proceedings Supplements* **150** (2006). `https://doi.org/10.1016/j.nuclphysbps.2004.08.048`.

19. GEANT collaboration, *Geant4 User's Guide for Application Developers*, GEANT4 10.7 ed (2020).

20. C. Saint-Gobain, *BC400 BC404 BC408 BC412 BC416 Data Sheet* (2018).

21. A. Wieczorek, *Development of novel plastic scintillators based on polyvinyltoluene for the hybrid J-PET/MR tomograph* (2017).

22. S. Korpachev, and M. Chadeeva, *Geant4 simulation of optical photon transport in scintillator tile with direct readout by silicon photomultiplier* (2017).

23. Berkeley Nucleonics Corp *Radioactive Check Sources Alpha, Beta, Gamma and Mixed Isotopes* `https://www.berkeleynucleonics.com/check-source`.

24. Stanford Environmental Safe & safety *Na-22 Radionuclide Fact Sheet.* `https://ehs.stanford.edu/reference/na-22-radionuclide-fact-sheet`.

25. Stanford Environmental Safe & safety *Cs-137 Radionuclide Fact Sheet.* `https://ehs.stanford.edu/reference/cs-137-radionuclide-fact-sheet`.

26. Stanford Environmental Safe & safety *Co-60 Radionuclide Fact Sheet.* `https://ehs.stanford.edu/reference/co-60-radionuclide-fact-sheet`.

27. Stanford Environmental Safe & safety *Sr-90 Radionuclide Fact Sheet.* `https://ehs.stanford.edu/reference/sr-90-radionuclide-fact-sheet`.

28. S.-G. Crystals, *LYSO Scintillfigureation MAterial $Lu_{1.8}Y_{.2}SiO_5{:}Ce$* 2017.

29. C. H. Zepeda Fernández, Time Resolution Simulation Measurement for the Configuration Plastic Scintillator Material+SiPM and its Application to Medical Physics, *J. Phys.: Conf. Ser.* **540** (2020) 012031.

30. T. Sui, Z. Zhao, S. Xie, Q. Huang, J. Xu and Q. Peng, Pico-TDC: a novel FPGA-based TDC with 2.2ps RMS timing resolution. *2017 IEEE Nuclear Science Symposium and Medical Imaging Conference (NSS/MIC)* 2017 `10.1109/NSSMIC.2017.8532955`

31. Ayala-Torres *et al.*, Performance of BeBe, a proposed dedicated beam-beam monitoring detector for the MPD-NICA experiment at JINR, *Journal of Instrumentation* **17** (2022) P09031.

32. Niedźwiecki *et al.*, J-PET: a new technology for the whole-body PET imaging, *Acta Phys. Polon. B* **48** (2017).